JOURNAL OF THE KOREAN ASTRONOMICAL SOCIETY
31: 1 ~ 17, 1998

DYNAMICAL CHARACTERISTICS OF THE QUIET TRANSITION REGION: SPATIAL CORRELATION STUDIES OF H I 931 AND S VI 933 UV LINES

YUN, HONG SIK [1], CHAE, JONG CHUL [2] AND POLAND, A. I.[3]
[1]Department of Astronomy, Seoul National University, Seoul 151-742
[2]Big Bear Solar Obervatory, New Jersey Institute of Technology, Big Bear City, CA 92314-9672
[3]Laboratory for Astronomy and Solar Physics, NASA/Goddard Space Flight Center, Greenbelt, MD 20771
(Received Jan. 7, 1998; Accepted Feb. 13, 1998)

ABSTRACT

To understand the basic physics underlying large spatial fluctuations of intensity and Doppler shift, we have investigated the dynamical charctersitics of the transition region of the quiet sun by analyzing a raster scan of high resolution UV spectral band containing H Lyman lines and a S VI line. The spectra were taken from a quiet area of $100'' \times 100''$ located near the disk center by SUMER on board SOHO. The spectral band ranges from 906 Å to 950 Å with spatial and spectral resolution of $1''$ and 0.044 Å, respectively. The parameters of individual spectral lines were determined from a single Gaussian fit to each spectral line. Then, spatial correlation analyses have been made among the line parameters. Important findings emerged from the present analysis are as follows.

(1) The integrated intensity maps of the observed area of H I 931 line (1×10^4 K) and S VI 933 line (2×10^5 K) look very smilar to each other with the same characterstic size of $5''$. An important difference, however, is that the intensity ratio of brighter network regions to darker cell regions is much larger in S VI 933 line than that in H I 931 line.

(2) Dynamical features represented by Doppler shifts and line widths are smaller than those features seen in intensity maps. The features are found to be changing rapidly with time within a time scale shorter than the integration time, 110 seconds, while the intensity structure remains nearly unchanged during the same time interval.

(3) The line intensity of S VI is quite strongly correlated with that of H I lines, but the Doppler shift correlation between the two lines is not as strong as the intensity correlation. The correlation length of the intensity structure is found to be about $5.7''$(4100 km), which is at least 3 times larger than that of the velocity structure.

These findings support the notion that the basic unit of the transition region of the quiet sun is a loop-like structure with a size of a few 10^3 km, within which a number of unresolved smaller velocity structures are present.

Key Words : Transition region, Dynamical characteristics, UV Lines, Velocity structure, Loop-like structure

I. INTRODUCTION

One of the puzzles in the solar physics is that most UV lines formed in the transition region appear predominantly redshifted (Doschek, Feldman & Bohlin 1976; Gebbie et al. 1981; Dere, Bartoe & Brueckner 1984 ;Rottman et al. 1990). If observed redshifts could be attributed to the net downward flow, they would create a serious problem in mass balance in the outer atmosphere of the sun. The flow would drain out all the material in the corona in a few hours so that the corona would not exist, thus contradicting the nature. Therefore, it is evident that the predominant redshifts should not be interpreted as being due to net downward mass flow. This is the reason why the observed redshifts are frequently interpreted as a selection effect which may be resulted from weighted averaging

process of line profiles over spatially and temporarily unresolved dynamical features.

A number of different physical models have been proposed to account for the selection effect leading to the observed redshifts. They include steady flow through spatially unresolved loops (e.g., McClymont 1989; Chae, Yun & Poland 1997) and compressive waves driven either from the chromosphere (Pneuman & Kopp 1978; Athay 1987; Cheng 1992) or from the corona (Hansteen 1993). McClymont (1989) showed that steady flow in cool loops driven by the buoyancy force set up by a small heating asymmetry between two legs of the loop offers a possible explanation. According to this model, both the temperature and the magnitude of flow velocity have peak values at the downflowing part of the loop. As a result, the emission-weighted Doppler shift has a value of 5 km/s at $T = 10^5$ K, which is close to the observed one.

Chae, Yun & Poland (1997) calculated a set of flux tube models with steady downflow and upflow. Their model shows that the enthalpy transported from the corona by downward flow is important in determining the thermal structure of the transition region and makes the transition zone broader than that with upward flow, resulting in increase in the emission measure. They interpreted the predominant redshift as a selection effect occurring when unresolved downflow and upflow regions with different emission measures are spatially averaged.

Cheng (1992) simulated a spicule with a single quasi-impulsive wave generated at the low chromosphere and showed that the observed downflow at $T = 10^5$ K is a direct result of the spicular upflow. According to this model, when the material moves upward, the density becomes high and the flow velocity is low, while when the material returns downward through the same region the density becomes low and the velocity is high. Consequently, even though the time-averaged mass flux is zero, there remains a net downward value in the time-averaged velocity. Hansteen (1993) considered a hypothesis that downward propagating compressive waves with origin in coronal nanoflare can account for the pervasive redshift. He found two effects contributed to the redshift, namely the particle motion in the acoustics wave coupled with the line emission and the physical displacement of the transition region itself.

To assess each of these models, we need to establish more observational characteristics of the transition region lines. One of the important observational establishment is variations of the observed average redshift and non-thermal broadening with temperature. According to the recent study made by Chae, Yun & Poland (1998), the average redshift at the base of the transition region is about 1-2 km/s, increasing with temperature with a peak value of 11 km/s near 2.3×10^5 K and then it decreases but remain still above zero(e.g., 5 km/s in Ne VIII line and 4 km/s in Mg X lines). As in the case of the redshift, the non-thermal velocity also increases with temperature, starting from values smaller than 10 km/s at temperatures below $T = 2 \times 10^4$ K to reach a peak value of 30 km/s around $T = 3 \times 10^5$ K, and then decreases with temperature, with the coronal velocity of about 20 km/s (Chae, Schühle & Lemaire, 1998). It is noteworthy that the nonthermal velocity associated with the line broadening ranges from 10 to 30km/s, which is larger than the Doppler velocity associated with the redshift ranging from 0 to 10 km/s.

An important question to be resolved is whether there exists any correlation among line profile parameters such as line intensity, shift and width. A positive correlation between line intensity and redshift has been reported by some studies (Gebbie et al. 1981; Athay & Dere 1991; Henzel & Engvold 1992), while other studies found no such correlation (Athay et al. 1983; Dere, Bartoe & Brueckner 1984). There is also some dispute in correlation between line width and intensity or between line width and redshift. Athay et al. (1983) found a correlation between redshift and width, all but with a lack of correlation between intensity and width. On the contrary, Dere, Bartoe & Brueckner (1984) reported a strong correlation between intensity and width. At present the reason why there exists such disagreement is not clear. It may be due to the difference in observing features and spatial resolution (Athay & Dere 1991) or systematic errors which may exist in measurements of line parameters (Dere, Bartoe & Brueckner 1984). Large intrinsic spatial variations of line parameters will also make it difficult to derive any solid answer to this problem.

We expect that SUMER(Solar Ultraviolet Measurement of Emitted Radiation) on board of SOHO (Solar Heliospheric Observatory) may provide a better understanding of the physical processes leading to line broadening and redshift, for SUMER is superior to previous UV experiments in several aspects (Wilhelm et al. 1995, 1997; Lemaire et al. 1997). It can measure any UV line in the wavelength ranging from 660 Å to 1610 Å in the 1st order with a spectral resolution of 45 mÅ per a detector element and from 330 Å to 805 Å in the 2nd order with a spectral resolution of 22 mÅ per a detector element. It has very good imaging capabilities, making it possible to obtain raster maps of line parameters with spatial resolution up to $1''$. A large amount of observational data obtained

from uninterrupted and long-lasting operation of the instrument enables us to study statistical properties and time variations of dynamical features seen by various UV lines.

In the present work we have investigated dynamical characteristics of the quiet sun based on the observations made by SUMER. Firstly we address to the question whether there is any correlation among line parameters by analyzing the obsevered spectra of H Lyman lines and a S VI line. The spectral band containing these lines has a great advantage of accurately calibrating wavelengths since the band includes several O I lines which can be used as reference lines.

II. OBSERVATION

An EUV spectroscopic observation of a quiet region was made by SUMER at 11:28 UT on July 23, 1996. The observed area has the size $100'' \times 100''$ and is located at $18''$ eastward and $180''$ northward from the disk center. No active features were found around the observed area in any of synoptic BBSO H α, Kit Peak He I 10830 and SOHO EIT images. Therefore, we believe that the observed area is truly representing a quiet sun at the solar minimum. The raster scan of the observed area was made by shifting successively the center position of the slit 4 ($1'' \times 120''$) toward the east with a step size of $1.14''$. The incident light over the detector was integrated for 110 seconds at each slit position and it took 3 hours and 20 minutes for the whole scan.

The spectral range covered in the present study is from 906 Å to 950 Å where a number of Lyman lines and S VI 933 line can be found. The spectral range also includes a number of O I lines which can be used as references for wavelength calibration. A thorough list of line identification in this range is found in Wilhelm et al. (1997).

III. DATA REDUCTION AND ANALYSIS

Figure 1 shows the spectral region we analyzed in the present study. We measured the intensity, shift, and width of the lines H I 926, H I 931, and S VI 933 where wavelength calibration was made by taking the lines O I 925, O I 930 and O I 936.6 as references. The laboratory wavelengths of these lines were taken from Wilhelm et al. (1997).

(a) Line Fitting

We first derived the line center and width in detector pixel unit and the line intensity in event count on the detector, and then we converted the parameters into physical units after wavelength and intensity calibrations were made. We applied a Gaussian fit

$$I_i = I_{peak} \exp(-(\frac{\lambda_i - \lambda_c}{\Delta\lambda_D})^2) \quad (1)$$

to individual line profiles in order to determine the line parameters. For this purpose only a small spectral region containing each line was taken from the whole spectrum. The subspectrum was subtracted by a background continuum level and then the count value at the spectral part far away from the measured line was set to be zero to minimize the error due to adjacent lines. After then the accumulated count at every pixel was calculated by integrating the measured count from the left end pixel to the next pixel on the right successively. Since the accumulated count at the right end is just the total count in the line, we have taken the final count as total line intensity. The pixel value at which the accumulated count is equal to the half of the total count is defined as line center position. In order to ensure subpixel accuracy in the determination of the center position, we have linearly interpolated the center position value from the values at discrete pixels. The Gaussian width of the spectral profile is inferred from two pixel values, where the accumulated count becomes 1/4 and 3/4 of the total count, respectively. Our approach for a Gaussian fit is straightforward and does not need any iteration required in most non-linear fitting algorithms. Thus it is possible to perform the Gaussian fitting of the spectral line profile at every spatial point simultaneously with the help of computer software such as IDL which supports a vectorization of programming. This reduces drastically the computing time required to get maps of line parameters. The moment method (e.g. Dere, Bartoe & Brueckner 1984) for getting line parameters is also straightforward and conceptually simple. However, we found from experiments that this approach is so sensitive to the wing part of a spectral line that any spectral features adjacent to the measured line could produce a systematic error in determining the line center position and the line width.

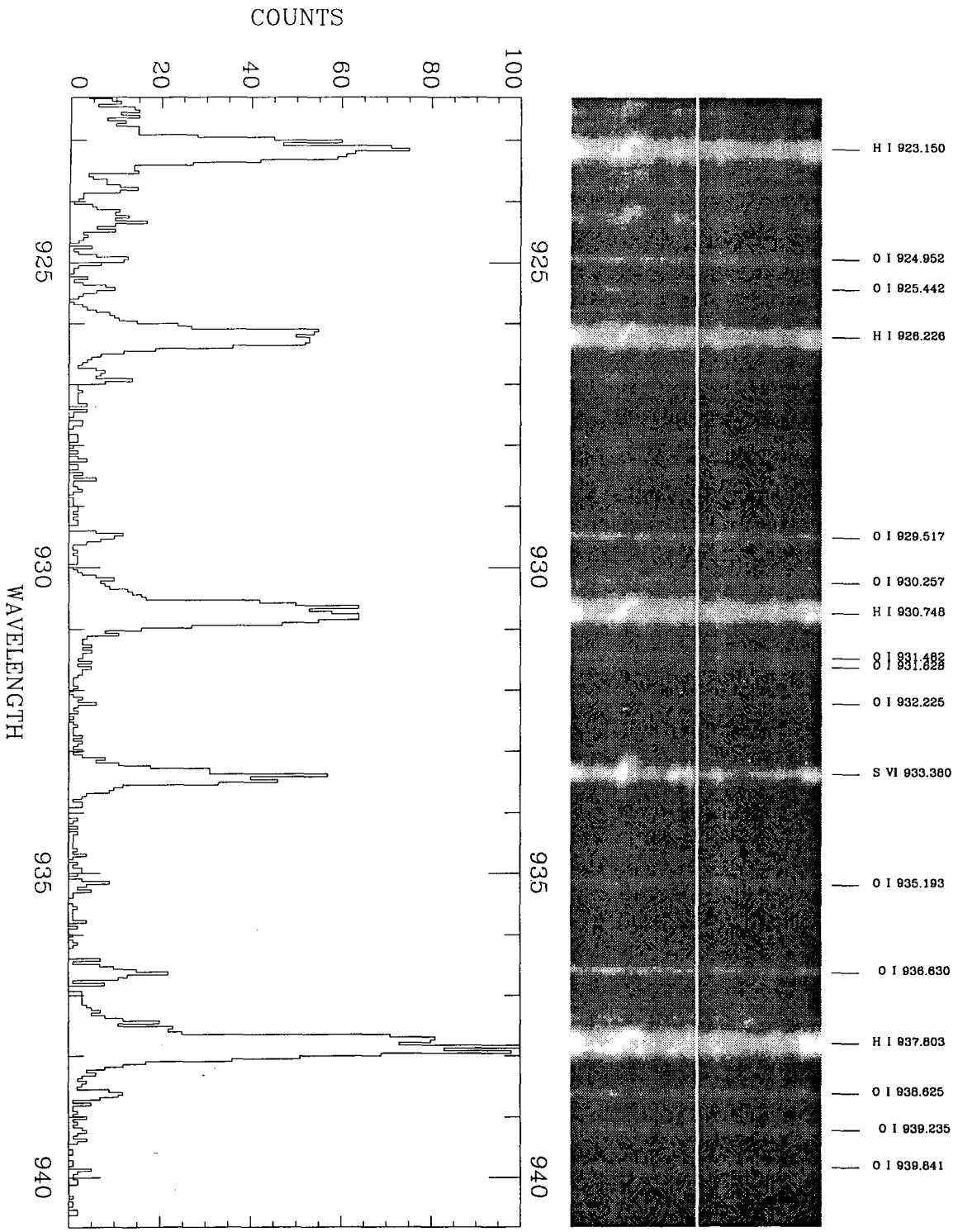

Fig. 1. An example of the spectrum obtained at the wavelength range including H I and S VI 933 lines.

(b) Wavelength Calibration

Regrettably, a spectrum image of the slit has some distortion both in wavelength direction and spatial direction due to the imperfectness of the detector. The amount of image distortion is smallest at the central part of the detector and increases with the distance from the detector center. Since our observation was made by choosing slit 4 which forms its image with length 120″ around the central row of the detector, the distortion along the spatial direction may be neglected. Moreover, it is found that determination of line intensity and width is nearly free from image distortion. Therefore, we applied a correction only to the line center position for the distortion along the wavelength direction with the help of the table provided by Moran (1996, 1998). The table gives the deviation of the line center position in detector pixels from the expected one as a function of the position on the detector. The correction of the line center position turned out to be trivial.

Once the distortion correction was made for the line center position, we calibrated the wavelength of the spectrum. Since three O I lines are available in the spectral range of our interest, we divided our spectral range into two parts, one from O I 924.952 to O I 929.517 and the other from O I 929.517 to O I 936.630. The conversion from the detector pixel value to the wavelength is achieved by adopting a linear relation between them in each part. Since O I lines have much smaller counts than Lyman and S VI lines, there may be present some error in positioning the line center. Therefore, we have taken an average of the O I line center positions along the spatial direction to get more accurate line center position, which in turn yields more accurate dispersion. For every slit image obtained by the raster scan the same process was repeated for wavelength calibration. As a result we have obtained reliable maps of absolute Doppler shift as well as line width over the observed area.

(c) Errors in Line Parameters

There may be a systematic error in the measured line parameters, but it is not well understood at the present time so that it is very difficult to estimate systematic errors. However, an error occurred from random noise can be easily estimated only if we know the noise characteristics of the observing system. We have examined the dependence of the noise on the signal from the Lyman continuum part in the wavelength raninge from 880 Å to 910 Å. This part has only a few visible lines and the continuum which is slowly increasing with wavelength, making it possible to separate signal from noise. We get the signal from the linear fit to the continuum and the noise from the residual. Figure 2 presents the variation of noise as a function of signal we obtained from a number of observations made through Lyman continuum. It is noted that the variation of signal is not due to the intrinsic variation of the sun, but it is nothing but a reflection of the difference in the integration time. We find that the signal with count less than 100 has a noise which is nearly equal to square root of the signal. On the other hand, the signals with count having more than 100 has a noise which is proportional to the signal itself. The noise characteristics at the low signal part is just what we expect from Poisson statistics. The reason why the noise is proportional to the signal at the high signal part is not clear. It could be due to the multiplicative error introduced by the uncertainty in flat field correction of the detector.

In the present study, the count is usually less than 100 so that we may assume safely that the noise is equal to the square root of the signal. We also assume that the line parameters obtained from Gaussian fitting are equal to those obtained from the moment method. This assumption is valid as far as the fitted line is well separated from other lines and has a very small continuum level. Then, the errors in line parameters may be easily calculated from the explicit formulae for the intensity, line center position, and line width as given in the moment method by doing error propagation analysis.

The results are

$$\epsilon(I) = \sqrt{I} \tag{2}$$

for line intensity I,

$$\epsilon(\lambda) = \Delta\lambda_D/\sqrt{2I} \tag{3}$$

for line center position λ and

$$\epsilon(\Delta\lambda_D) = \Delta\lambda_D/\sqrt{I} \tag{4}$$

for Doppler width $\Delta\lambda$.

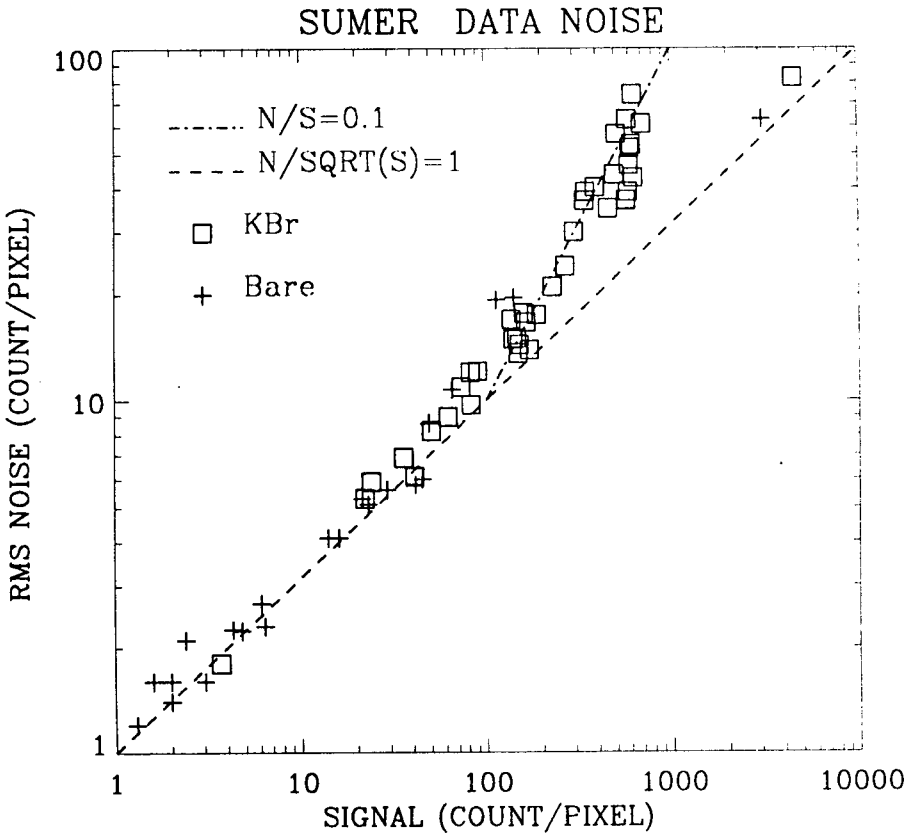

Fig. 2. Noise characteristics of SUMER observing system.

It is interesting to note that the errors associated with estimating the line center position and the line width depend on intensity as well as the line width. In spatial regions where the intensity is roughly equal to the spatial average of the quiet sun intensity, the error in intensity is estimated to be about 10 % for O I lines, 4 % for Lyman lines and 5 % for S VI 933 line. The estimated error in the line center is about 8.5 mÅ (2.7 km/s) for O I lines, 5 mÅ (1.6km/s) for Lyman lines and 5 mÅ (1.5km/s) for S VI 933 line. The error associated with the line width is larger than that with the line center by a factor of 1.4.

Even though the error in the line center of O I lines is rather large because of their low intensity, there is no difficulty of getting more accurate wavelength scale because we have taken an average of line center positions over the 100 spatial pixels. The error in wavelength calibration is estimated to be about 1 mÅ (0.3km/s).

IV. RESULTS

(a) Spatial Distribution of Line Parameters

i) Integrated Line Intensity

Figure 3 shows the intensity maps of S VI 933 and H I 931 lines, respectively. The data in dark columns on the figures were lost due to the telemetry problem. For comparison, we have overplotted the contours representing the average level of S VI 933 line on both figures, which mark the boundary between brighter network regions and darker cell regions. We also provided the gray scale of the logarithmic intensity at the top of each figure.

We find from the figures that gross intensity features seen in S VI line and H I line look very similar to each other and quite normal as expected in the quiet sun. One of the differences between the two maps is a bright patch

near the point x=62 and y=32 in S VI line map, which is absent in H I line map. We also note that the network to which this bright patch belongs is the brightest in both the maps. The most outstanding difference, however, is the difference in the intensity contrast between network regions and cell regions. Namely, the contrast in S VI intensity map is much larger than that in H I intensity map. The cell regions looks much darker in S VI map than in H I map. As a consequence, the average value of S VI intensity is smaller than that of H I intensity. This difference is illustrated in Figure 4 where the number distribution of the logarithmic value of intensity in the observed area is presented for H I line and S VI line.

ii) Doppler Shift

Figure 5 displays the Doppler velocity maps of S VI line and H I lines, where a positive value of velocity means redshift or downflow. Since the overplotted contours are the same as used in the intensity maps (see Figure 3), we can easily match any features found in the velocity maps with those in intensity maps. It is clear from the figures that large values of redshift are mostly found in network regions and cell regions have smaller redshifts or blueshifts in both H I 931 and S VI 933 lines. Therefore it is expected that there is a positive correlation between Doppler velocity and intensity. An interesting characteristic found in the velocity maps is that there exist features with large blueshifts. They are found anywhere in the quiet sun, but there is a great tendency that they occur near the boundary between network regions and cell regions. The number distributions of Doppler velocity in the same observed area are given in Figure 6. One of the most important observational parameters we have obtained from the present study is the average Doppler velocities of H I lines and S VI line in the quiet sun. We find that the average Doppler velocity is 9.4 km/s in S VI line and 0.9 km/s in H I 931 line. We believe the error in determining the average Doppler velocity is within 0.5km/s.

Another important observational parameter is the standard deviation of the Doppler velocity from the average value. H I 931 line has a standard deviation of 4.1 km/s, and S VI 931 line, 5.0 km/s. Since these values are larger than the error in estimating Doppler velocity, they may be regarded as a manifestation of large intrinsic spatial variations of Doppler velocity on the observed area. This view is fully consistent with the previous authors and leads us to search for physical cause of such large fluctuations in Doppler velocities.

It is also noted that the variation of Doppler velocity from pixel to pixel is much larger than the error in estimating the parameter. This suggests that basic structures giving rise to the observed Doppler shift is smaller than our resolution element $1''$, supporting the hypothesis that the upper atmosphere is made up of fine scale structures. It appears that the variation from pixel to pixel is larger in cell regions than in network regions. At present we are not sure whether this trend is real or not because much smaller intensity in the cell regions may lead to increase in the error of the measured Doppler shifts. If it should turn out real, it means that cell regions have more complex small scale structures than network regions.

iii) Doppler Width

Figure 7 shows the Doppler width maps of S VI line and H I line. As can be seen from the figures, we find that network regions usually have larger width than cell regions. However, as noted from Figure 5, the largest widths are not found in network regions, but in those regions with large blueshifts. This is because blue shift features display spectral profiles with two or more components. It is likely that these blue-shifted features with large line widths represent transition region explosive events. If then, their locations are consistent with Chae et al. (1998c)'s finding that transition region explosive events occur preferentially at weak and mixed polarity flux regions which are away from strong network magnetic flux concentration. Except for the blueshift features, it is very likely that there exists a positive correlation between line width and line intensity in S VI line. In H line, however, larger values of line width are frequently found also in cell regions as well as in network regions so that it becomes very hard to establish any correlation between intensity and width. The fact that H lines are not optical thin and subject to the Stark broadening also adds to the difficulty in interpreting the spatial distribution of H line width.

The number distributions of Doppler width in the same area are presented in Figure 8. The average line widths of these two lines are found to be 117 mÅ(S VI line) and 186 mÅ(H I line), which are found to be rather large. We attribute the large Doppler width in the H line to the fact that H lines are subject to Stark broadening and they are not optically thin. The standard deviations of the distribution of Doppler width are 20 mÅ and 15 mÅ , respectively.

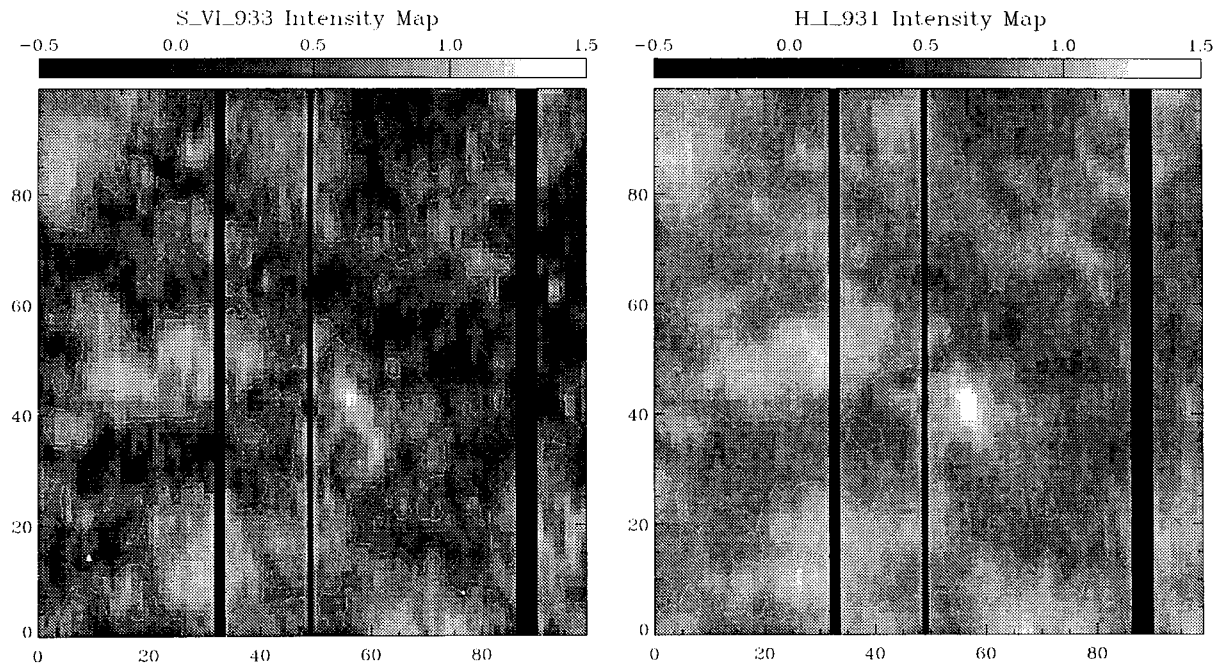

Fig. 3. Intensity maps of S VI 933 and H I 931 lines with a gray scale of logarithmic intensity in unit of erg cm^{-2} s^{-1}. The contours represent the average level of S VI line intensity, which separates brighter network regions from darker cell regions.

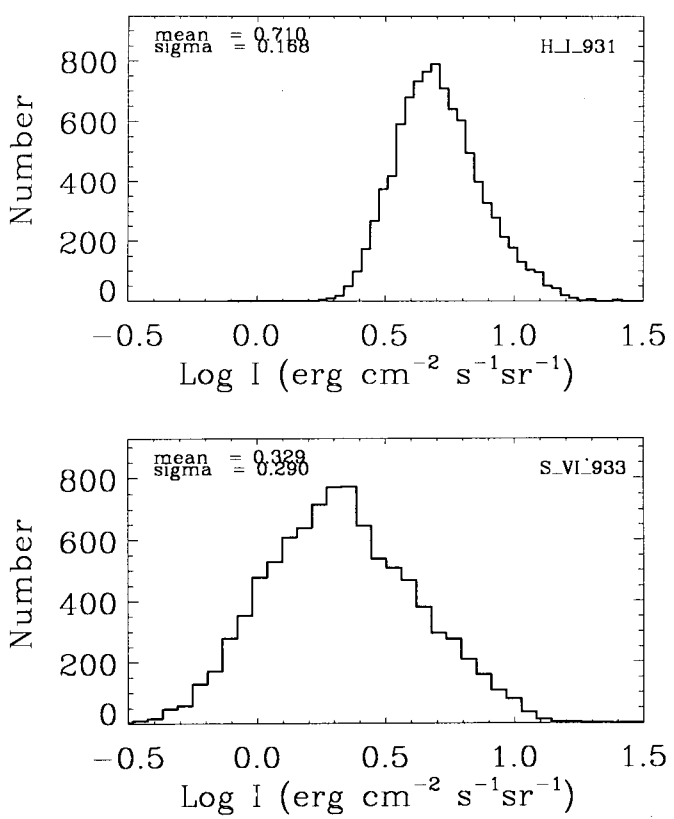

Fig. 4. Number distribution of H I 931 and S VI 933 line intensities in the quiet sun.

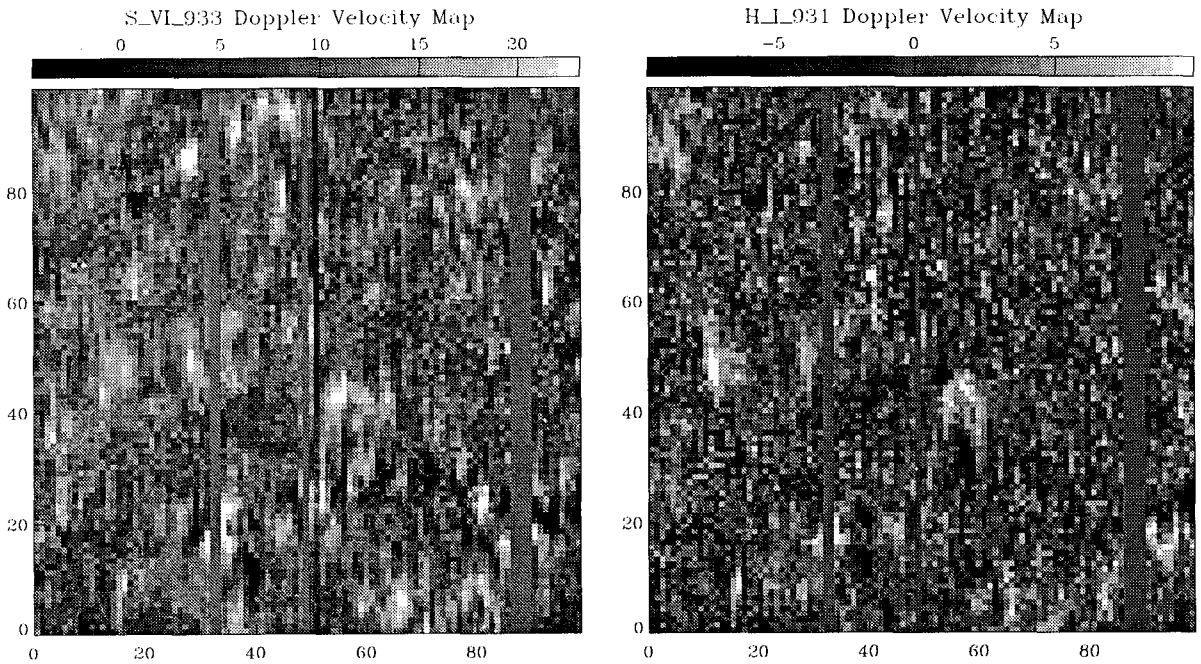

Fig. 5. Doppler shift maps of S VI 933 and H I 931 lines. The scales on the tops are in unit of km s^{-1}. The contours represent the average level of S VI line intensity, which separates brighter netwrok regions from darker cell regions.

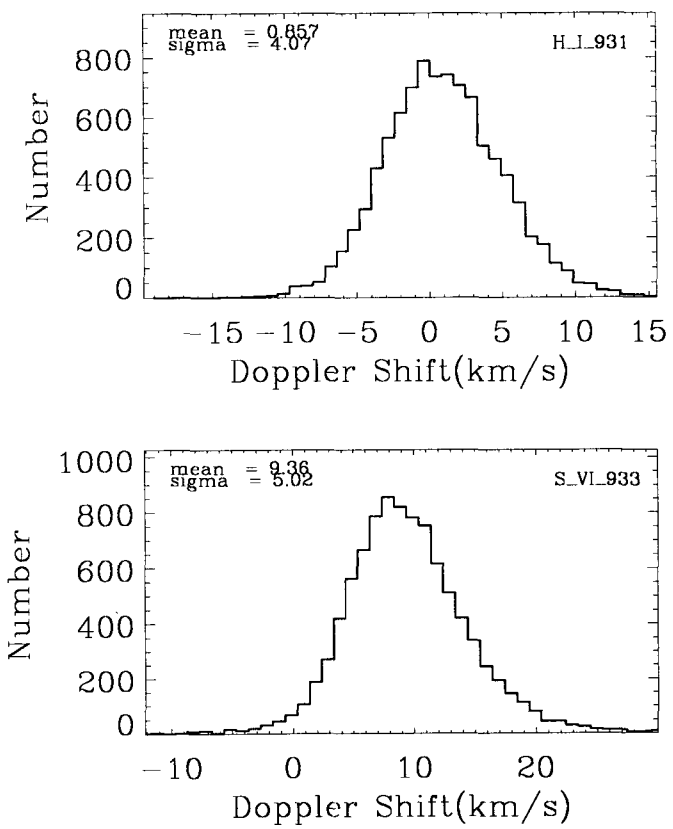

Fig. 6. Number distribution of H I 931 and S VI 933 Doppler shifts in the quiet sun

They are larger than the measurement error of the line width. Consequently, they represent intrinsic fluctuations of line width over the observed area.

(b) Correlations among Intensity, Shift and Width

To understand the basic physics underlying large spatial fluctuations of intensity and Doppler shift, we have examined their spatial autocorrelation and correlation analyses among the line parameters of the two UV lines, H I and S VI lines. The resulting line intensity correlation and Doppler velocity correlation between the two lines are presented in Figure 9 and Figure 10, respectively. As seen from the figures the line intensity correlation between the two lines is strongly correlated (with a correlation coefficient of 0.85), but the Doppler shift correlation is not as strongly correlated as the line intensity correlation (with a correlation coefficient of 0.25). A similar correlation analyses have been made between line intensity and Doppler shift for the two lines. The results are shown in Figure 11, where it is noted that both lines have a positive correlation between line intensity and Doppler shift with a correlation coefficient of about 0.35. We have also examined the correlation between line intensity and width. The resulting correlations are shown in Figure 12. As seen from the figure, H line shows extremely weak or nearly no correlation between line intensity and width, but S VI line has rather weak correlation. Since S VI line has some positive correlations between intensity and Doppler shift and between intensity and width, we have examined the correlation between width and shift of S VI line. The resulting correlation is shown in Figure 13, which shows a trend that the width increases with Doppler shift for the S VI line. Finally, a spatial autocorrelation study has been made to line intensity, Doppler shift and line width of S VI line, where two cases are considered depending on taking data along or across the slit. The resulting correlation studies for both cases are presented for S VI and H lines in Figure 14 and Figure 15, where solid, dotted and dashed lines refer to line intensity, Doppler shift and width, respectively. It is very intresting to note that the correlation length of the intensity structure is found to be about 5.5″(4100 km), which is at least 3 times larger than that of velocity structure. If we carefully examine Figure 14, we also see that the Doppler shift correlation length of the S VI line measured across the slit is about 1.5″ which is much smaller than the value of 3″ measured along the slit. The difference may be attributed to the time difference between adjacent exposures, during which period velocity structures may change. On the other hand, the intensity correlation lengths measured along and across the slit are about the same. This supports the notion that the basic unit of the transition region of the quiet sun is a loop-lile structure with a size of a few 1000 km, whithin which a number of unresolved smaller velocity structures are present.

V. SUMMARY AND CONCLUSION

In the present study we have examined dynamical characteristics of the upper atmosphere of a quiet sun through H I 931 line(1×10^4 K) and S VI 933 line(2×10^5 K) by examining correlation between intensity, shift and width in each line. The spectra have been taken with SUMER with a spatial resolution of 1″ and a spectral resolution of 0.044 Å per pixel. The data cover a spectral range from 906 Å to 950 Å in a quiet area of 100″ × 100″ located near the disk center. The wavelength scale has been calibrated in reference to narrow chromospheric O I 930 and 937 lines.

The line profiles and parameters have been determined from a single Gaussian fit to each spectral line. The probable errors in intensity and line shift measurements were found to be 5 % and 0.005 Å (1.5 km/s) for both lines. The spatial averages and standard variations of the line parameters over the observed area are summarized in the following table. Important findings emerged from the present analysis are as follows.

(1) The number distributions in logarithmic line intensity, Doppler shift and non-thermal line broadening are found to be nearly normal. Their spatial averages and associated variance have been estimated which are summarized below.

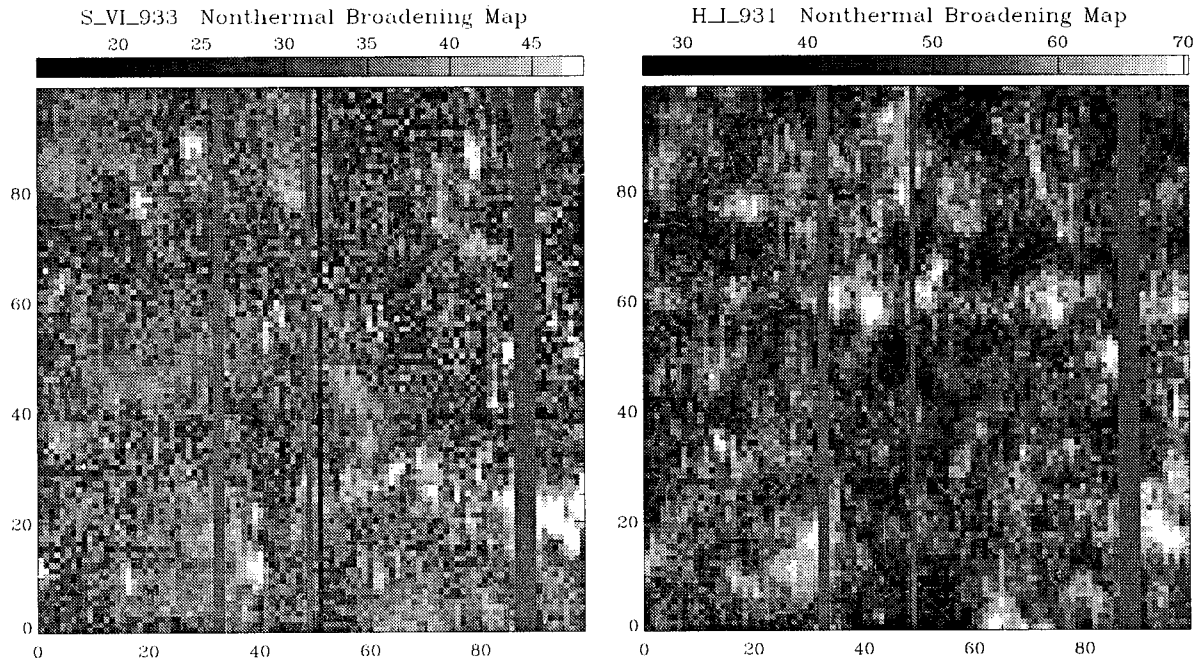

Fig. 7. Map of S VI 933 and H I 931 line widths in the quiet sun.

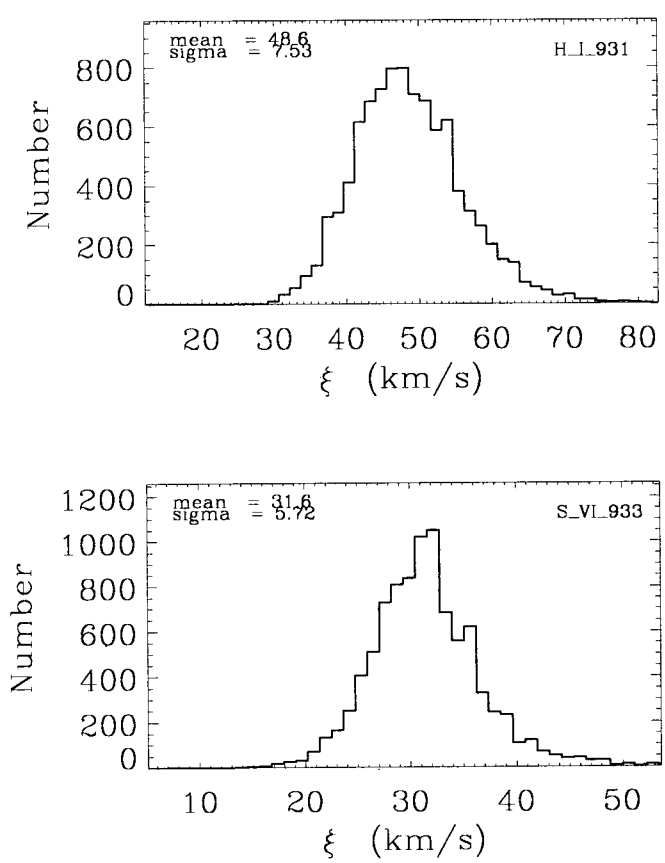

Fig. 8. Number distribution of H I 931 and S VI 933 line widths in the quiet sun.

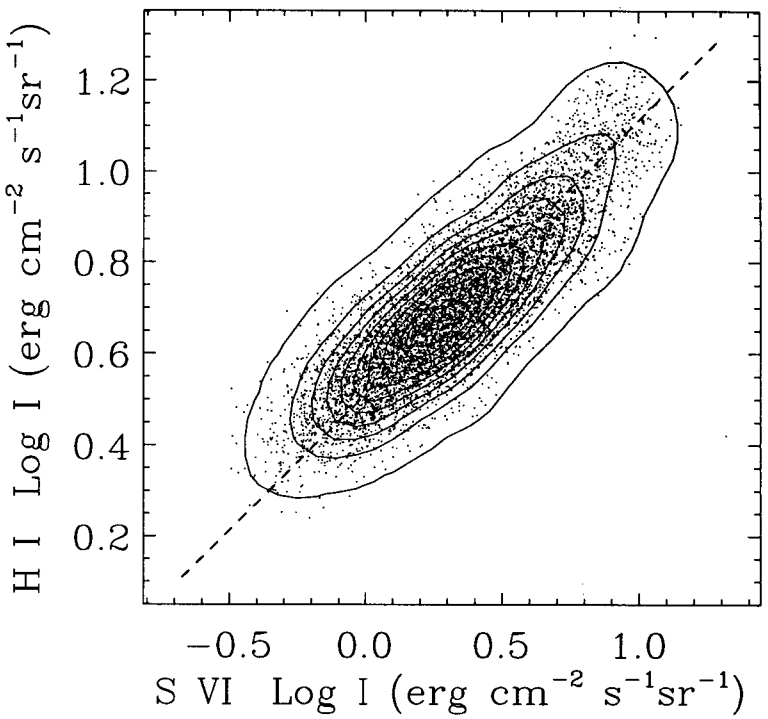

Fig. 9. Correlation between S VI and H I line intensities.

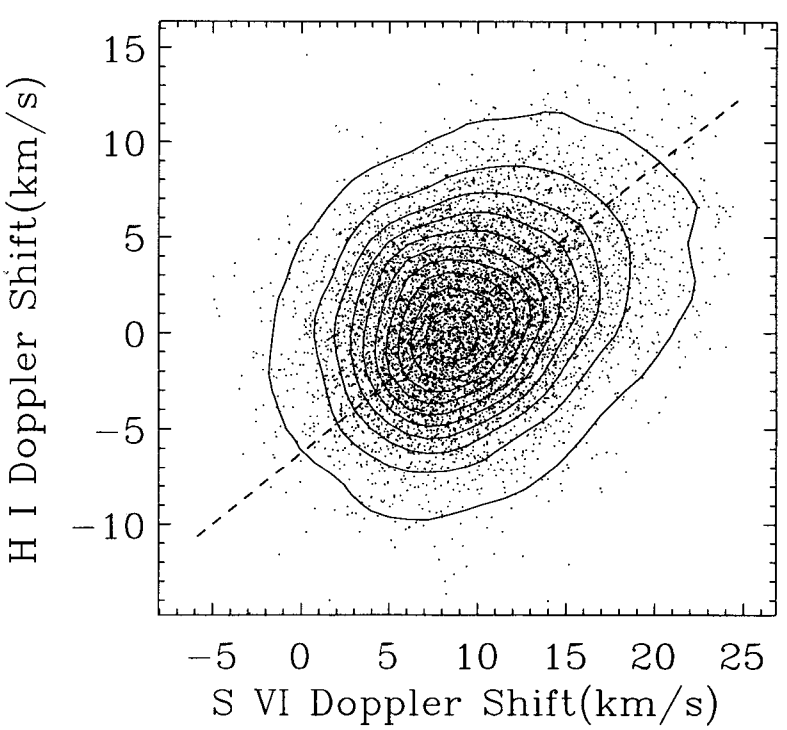

Fig. 10. Correlation between S VI and H I line Doppler shifts. The contours represent the number density of the data points on the plot to display the correlation.

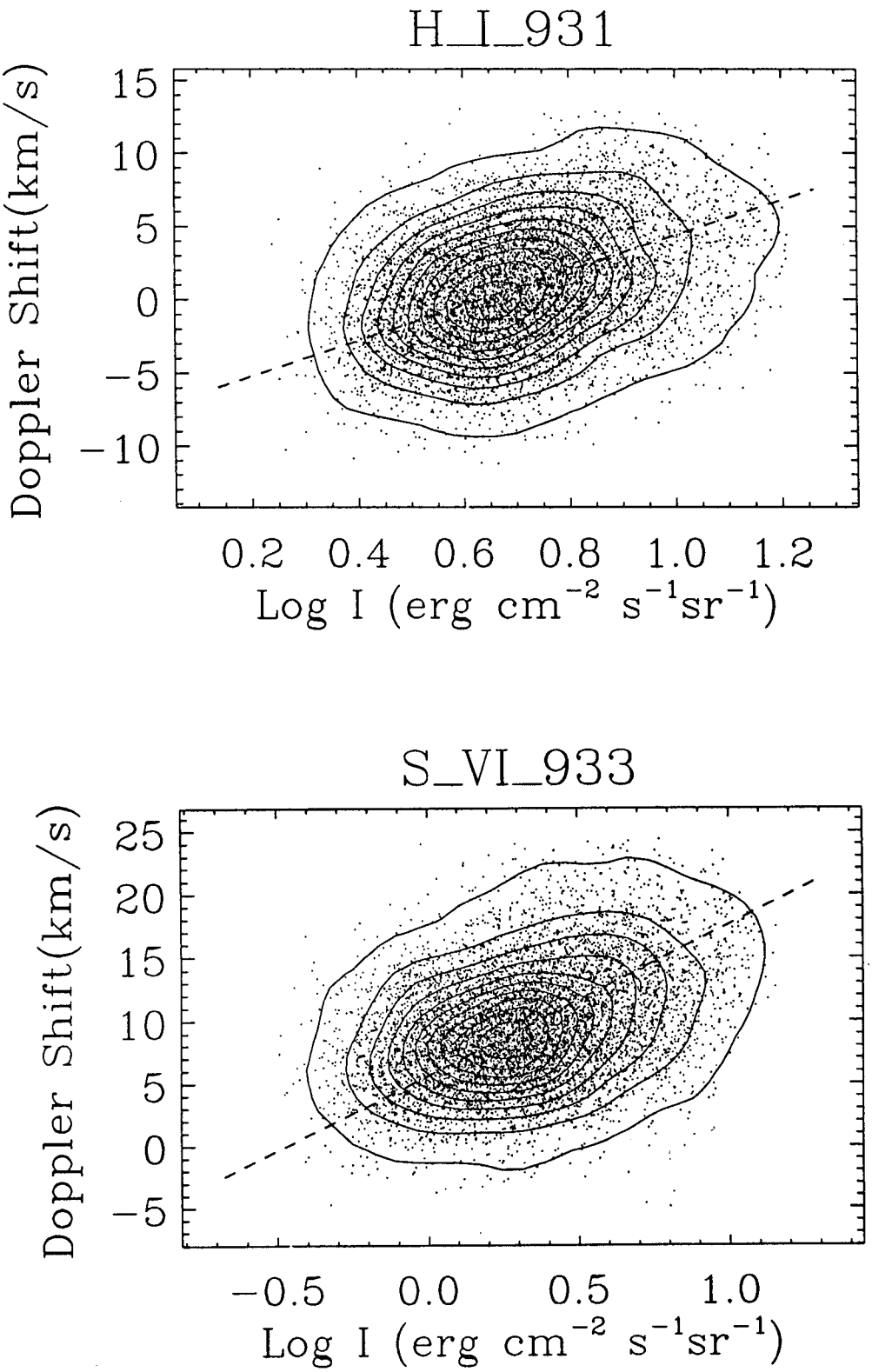

Fig. 11. Correlations between line intensity and Doppler shift.

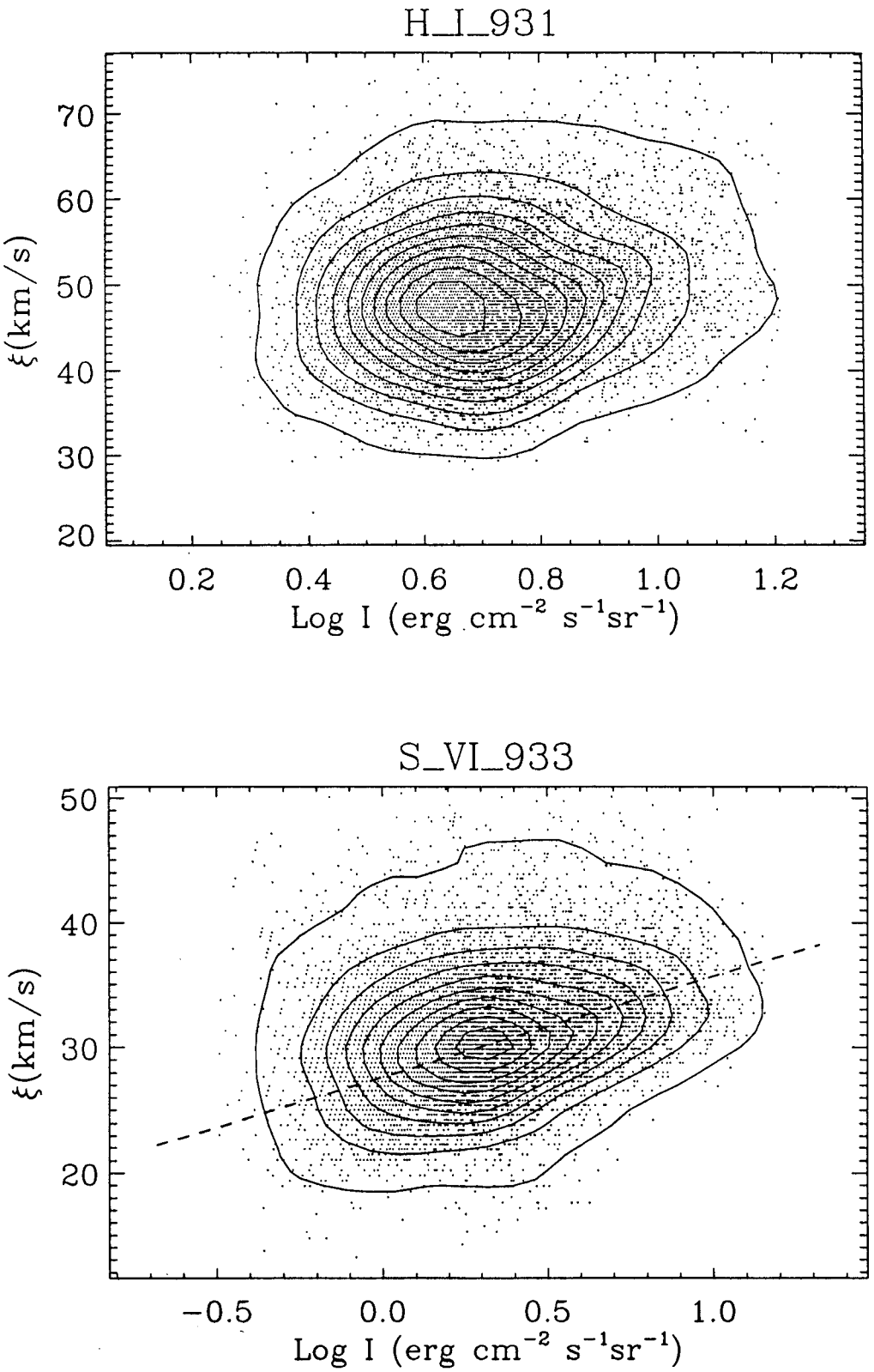

Fig. 12. Correlations between line intensity and line width.

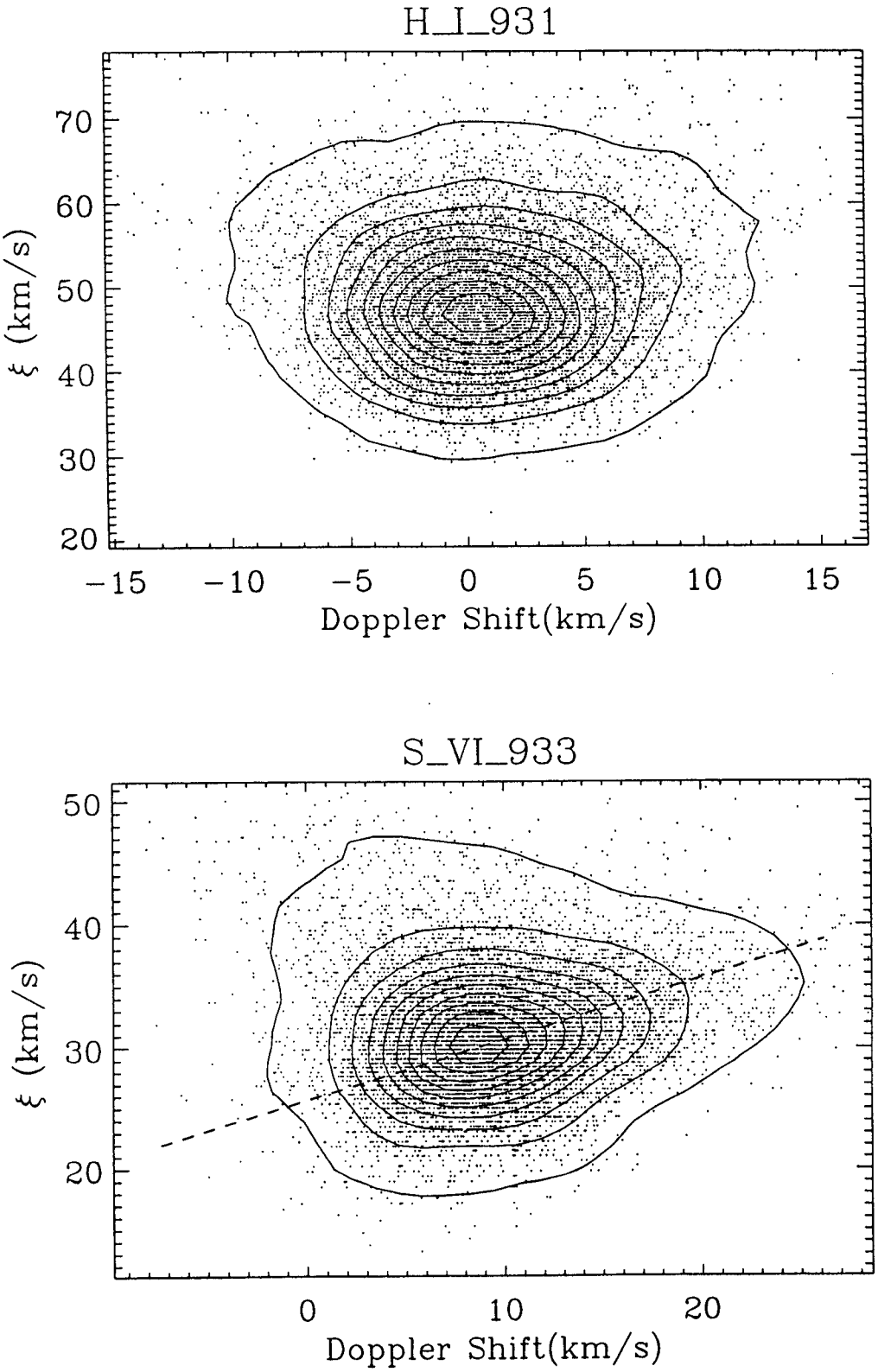

Fig. 13. Correlations between Doppler shift and line width.

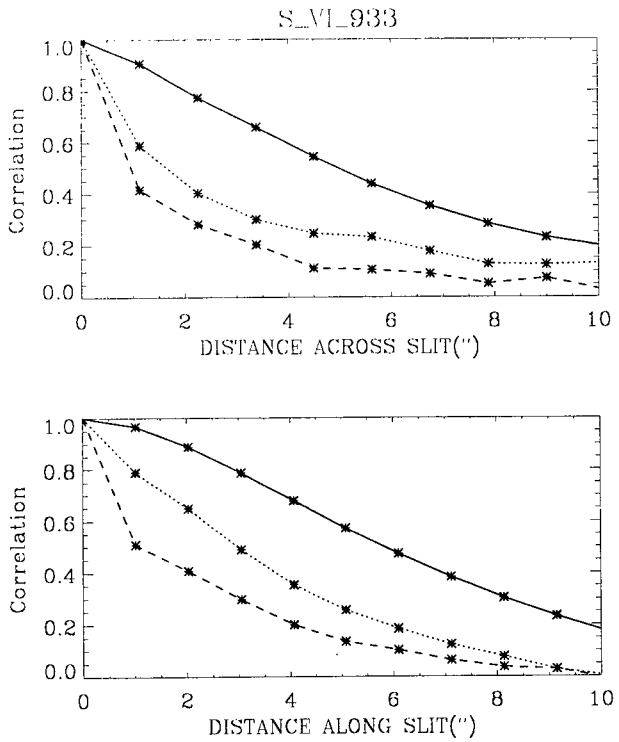

Fig. 14. Spatial autocorrelations of line intensity(solid), Doppler shift(dotted) and line width(dashed) of S VI line.

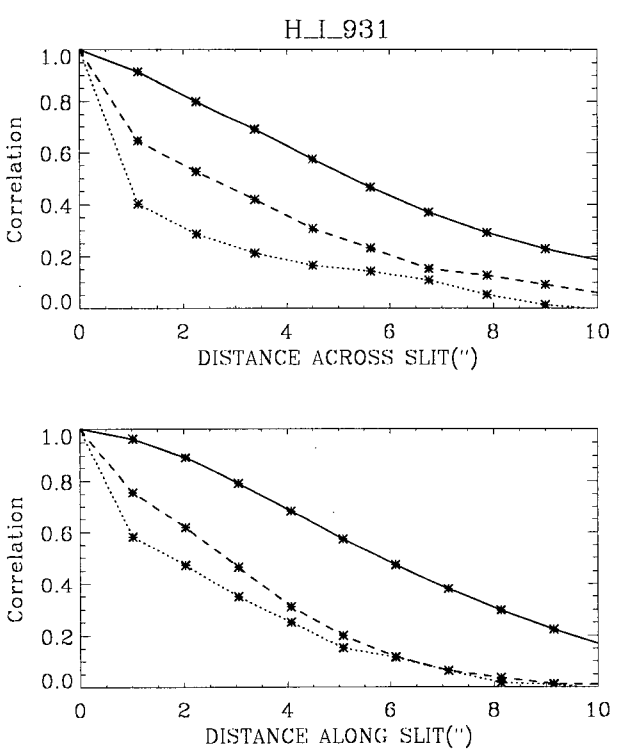

Fig. 15. Spatial autocorrelations of line intensity(solid), Doppler shift(dotted) and line width(dashed) of S VI line.

(2) The integrated intensity maps of the observed area obtained for H I 931 line (1×10^4 K) and S VI 933 line (2×10^5 K) look very smilar to each other. The average intensities of the quiet sun are measured to be 6.6 count/pixels/s for H I 931 line and 2.8 count/pixels/s for S VI 933 line. An important difference between H I 931 and S VI 933 line intensity maps is that the intensity ratio of brighter network regions to darker cell regions is much larger in S VI 933 line than that in H I 931 line, having value of 15 and 5, respectively.

(3) Dynamical features represented by Doppler shifts and line widths are found to be smaller than those features seen in intensity maps, which have charactertic size of $2''$ along the slit direction both in H I line and in S VI line. The smaller charcteristic size of $1''$ found along the scan direction indicates that the dynamical features are rapidly changing within the integration time of 110 seconds.

(4) The S VI line shows an average redshift of 9.5 km/s when measured from O I lines, while the H I line yields a spatial average of Doppler shift nearly equal to zero.

(5) The line intensity between the two lines is strongly correlated (with a correlation coefficient of 0.85), but the Doppler velocity is not as strongly correlated as the line intensity (with a correlation coefficient of 0.25). Both lines have a positive correlation between intensity and Doppler shift (with a correlation coefficient of 0.35).

(6) The velocity structure rapidly changes with time within a time scale shorter than the integration time, 110 seconds while the intensity structure remains nearly unchanged during the same time interval.

(7) The correlation length of the intensity structure is found to be about $5.7''$(4100 km), which is at least 3 times larger than that of velocity structure.

These findings support the notion that the basic unit of the transition region of the quiet sun is a loop-like structure with a size of a few 10^3 km, within which a number of unresolved smaller velocity structures are present.

ACKNOWLEDGEMENTS

We would like to thank the members of the SUMER team for technical support and T. Moran for providing the data for detector geometric distortion. One of us(H. S. Yun) expresses his sincere gratitude to A. I. Poland for support and hospitality during the stay at GSFC for 6 months in 1996. This work is partially supported by Korea-China Cooperative Project under NNSFC and KOSEF (966-0203-005-2) and by BSRI-97-5408. The SUMER project is supported by DLR, CNES, NASA, and the ESA PRODEX programme (Swiss contribution).

REFERENCES

Athay, R. G. 1987, Nature 327, 685
Athay, R. G., Gurman, J. B., Henze, W., & Shine, R. A. 1983, ApJ, 265, 519
Athay, R. G. & Dere, K. P. 1991 ApJ, 381, 323
Chae, J., Yun, H. S., & Poland, A. I. 1997, ApJ, 480, 817
Chae, J., Yun, H. S., & Poland, A. I. 1998a, ApJS, 114, 151
Chae, J., Schühle, U., & Lemaire, P. 1998b, ApJ(submitted)
Chae, J., Wang, H., Lee, C.-Y., Goode, P. & Schühle, U. 1998c, ApJ, 497, L109
Cheng, Q. Q. 1992, A&A, 263, 581
Dere, K. P., Bartoe, J.-D. F., & Brueckner, G. E. 1984, ApJ, 281, 870
Doschek, G. A., Feldman, U., & Bohlin, J. D. 1976, ApJ, 205, L177
Gebbie, K. B., et al. 1981, ApJ, 251, L115
Hansteen, V. H. 1993, ApJ, 402, 741
Henzel, W. & Engvold, O. 1992, Sol. Phys., 141, 51
Lemaire, P., et al. 1997, Sol. Phys., 170, 105
McClymont, A. N. 1989, ApJ, 347, L47
Moran, T., 1996, private communication
Moran, T., 1998, in preparation
Pneuman, G. W. & Kopp, R. A. 1978, Sol. Phys., 57, 49
Rottman, G. J., Hassler, D. D., Jones, M. D., & Orall, F. Q. 1990, ApJ, 358, 693
Wilhelm, K., et al. 1995, Sol. Phys., 162, 189
Wilhelm, K., et al, 1997, Sol. Phys., 170, 75